Finite Elements in Analysis and Design 47 (2011) 610–618

Contents lists available at ScienceDirect

Finite Elements in Analysis and Design

journal homepage: www.elsevier.com/locate/finel

Wavelet transformation based multi-time scale crystal plasticity FEM for cyclic deformation in titanium alloys under dwell load

Pritam Chakraborty *, Deepu S. Joseph, Somnath Ghosh

Department of Mechanical Engineering, The Ohio State University, Scott Laboratory, 201 West 19th Avenue, Columbus, OH 43210, United States

ARTICLE INFO

Article history:
Received 16 November 2010
Accepted 11 December 2010
Available online 5 January 2011

Keywords:
Wavelets
Multi-time
Titanium
Dwell
Fatigue
Micro-structure

ABSTRACT

Titanium alloys are used in high end applications due to their desirable properties. However under dwell fatigue loading, these alloys exhibit premature crack initiation and failure when compared to normal cyclic loading. This early crack initiation can be attributed to the inhomogenous plastic deformation occurring in these alloys during the hold period of dwell cyclic loading and is strongly influenced by the underlying micro-structure. This necessitates the consideration of micro-structural features and their influence on the response, for accurate life prediction in these alloys. Crystal plasticity based finite element simulations capture the micro-structural influence on the response and can prove effective for accurate prediction of crack initiation in these alloys. However 70–80% of total life in Ti-alloys based components is spent in crack initiation and this may involve crystal plasticity based finite element simulations for large number of cycles. Such simulations using conventional single scale time integration schemes can be computationally intractable. A multi-time scale method using wavelet based decomposition is thus developed in this work for accurate and computationally efficient dwell fatigue simulations of these alloys for large number of cycles.

1. Introduction

Titanium alloys are used in high performance applications due to their high specific strength, toughness and corrosion resistance at elevated temperatures. However these alloys exhibit premature failure under dwell cyclic loading when compared to normal cyclic loading [1]. The early failure is strongly influenced by the underlying micro-structure and the micro-structural influence on the response should be considered when dwell fatigue life analysis of these alloys are performed. The conventional lifing techniques, like the total life approaches or the damage or defect tolerance approaches [2], are macroscopic in nature and the micro-structural effects on fatigue life are captured empirically by shifts in data curves after extensive testing. In total life approaches, like the stress-life or the strain-life approach, the number of cycles to failure is determined from stress amplitude of loading (S–N curves) or from the accumulated plastic strain (Coffin–Manson rule) [3] respectively. In damage or defect tolerance approaches, fatigue life estimates are based on propagation of a pre-existing crack from an initial size to final failure. Models such as the Paris law [4] are employed together with fracture toughness or threshold stress intensity factors to determine the number of cycles to failure. Although these methods work well under specific testing conditions, they exhibit significant scatter in their predictions. When these lifing techniques are used to design Ti-alloys based components, a great number of them retires prematurely even before damage initiation, thus shortening their full useful life.

The micro-structure of Ti-alloys are strongly anisotropic which causes inhomogenous plastic flow and strain localization to happen, during the additional hold period at the maximum applied stress in dwell cyclic loading. This necessitates the consideration of micro-structural features and its influence on response variations for accurate life predictions in these alloys. The important micro-structural features that affect the dwell fatigue behavior in Ti-alloys are grain orientations, misorientations, size, shape and grain boundary defects. Crystal plasticity based material models are effective in capturing the micro-structural influence on response [5]. Ghosh and co-workers [6–10] have extended the crystal plasticity theories to model deformation and creep mechanisms in Ti-alloys (Ti-6Al, Ti-6242). The model considers the grain orientation and misorientation distributions, the grain size distributions and morphology, and has been used in this work. Crystal plasticity based finite element simulations of representative micro-structure of Ti-alloys under creep conditions show stress concentration at grain boundaries [9]. This stress concentration is the driving factor that causes premature crack initiation in Ti-alloys under dwell cycle loading [11].

Fatigue failure in polycrystalline alloys starts with crack nucleation followed by steady crack growth under cyclic stresses and final

* Corresponding author.
E-mail address: chakraborty.11@osu.edu (P. Chakraborty).

0168-874X/$ - see front matter © 2010 Elsevier B.V. All rights reserved.
doi:10.1016/j.finel.2010.12.014

failure due to crack coalescence [2]. In Ti-alloys 70–80% of total life is spent to initiate a crack and hence accurate estimate of number of cycles to crack initiation dictates the overall accuracy of predicted life. Crystal plasticity based finite element simulations in conjunction with a physically motivated crack initiation law can be used to accurately predict crack initiation in these alloys. However single time scale simulations for large number of cycles till crack initiation, employing conventional time integration schemes [12], can prove to be computationally prohibitive. In the single time integration schemes, each cycle is resolved into an appropriate number of time steps, over which integration is performed. In crystal plasticity calculations, a high resolution in the time steps is required for each cycle throughout the loading process, often leading to exorbitant computational requirements. Accelerated time integration schemes have been devised to perform the integration in an efficient manner for computational benefit.

Some of the existing accelerated time integration schemes are extrapolation based techniques, asymptotic expansion based methods and almost periodic temporal homogenization (APTH) operator based method. In extrapolation based methods [13–15], 3-D crystal plasticity simulations are performed for a small number of cycles and then the response variables are extrapolated to make fatigue life predictions. Extrapolation of local micro-structural variables can have considerable error and this can result in inaccurate prediction of number of cycles to crack initiation. The crystal plasticity variables display dual time scale characteristics under cyclic loading conditions, consisting of a high frequency oscillatory response (fine scale) and a low frequency monotonic response (coarse scale). This provides the basis to use temporal multiscale methods to decouple the coarse and fine scale response. The coarse scale response can then be integrated with larger time steps (in order of cycles) to attain significant computational benefit. Asymptotic expansion based methods and APTH operator based method falls under the category of multi-time scale methods. Asymptotic expansion based methods [16–18] assume scale separation and the crystal plasticity variables are expanded in an asymptotic series. The rate equations are modified based on different orders of contribution and integration of cycle-averaged variables are performed for computational benefit. These methods assume local periodicity or near periodicity and fails for reversible loading situations ($R\rightarrow -1$) where plastic oscillators are dominant. In APTH operator based method [19], almost periodicity of response variables are assumed and an operator is defined which satisfies the temporal periodicity condition in a weak sense for almost periodic variables. A staggered global–local approach is used to integrate the coarse scale variables for computational advantage. The strong non-linearity existing in crystal plasticity model for Ti-alloys makes the APTH operator based method to be unstable and hence cannot be used. The wavelet based multi-time scale method for cyclic simulations of polycrystalline alloys developed in [20] overcomes the drawbacks present in the existing accelerated time integration schemes. There is no assumption on the local periodicity of the variables and an implicit integration scheme is developed which is stable for strongly non-linear crystal plasticity model of Ti-alloys. This method is extended in the current work to perform finite element simulations of Ti-micro-structure under dwell fatigue loading with large time periods.

The organization of the paper is as follows. Section 2 describes the crystal plasticity model for Ti-alloys (Ti-6Al, Ti-6242). The existing accelerated time integration methods and their shortcomings are discussed in Section 3. The wavelet transformation based multi-time scale method is described in Section 4. Numerical results are presented in Section 5 to demonstrate the accuracy of the wavelet based method and also the ability to perform crystal plasticity based finite element simulations for large number of cycles. The paper is concluded in Section 6.

2. Crystal plasticity model for Ti-alloys

In crystal plasticity theory, the plastic deformation in polycrystalline alloys happens through slip on different slip systems [5]. The number of slip systems and their strength depends on the morphological and crystallographical characteristics of the micro-structure. Hence the micro-structural effect on the deformation of polycrystalline material is captured through crystal plasticity based models. The micro-structure of Ti-alloys (Ti-6Al, Ti-6242) is composed of primary α grains and transformed $\alpha+\beta$ colonies. The primary α grains have a hexagonal close packed (*hcp*) crystal lattice structure and is strongly anisotropic [6]. The transformed $\alpha+\beta$ colonies consist of alternate lathe of *hcp* lattice (α phase) and symmetric body centered cubic (*bcc*) lattice (β phase) [7]. The *hcp* crystal structure consists of three $\langle a\rangle$ basal slip systems $\{0\,0\,0\,1\}\langle 1\,1\,\bar{2}\,0\rangle$, three $\langle a\rangle$ prismatic slip systems $\{1\,0\,\bar{1}\,0\}\langle 1\,1\,\bar{2}\,0\rangle$, six $\langle a\rangle$ pyramidal slip systems $\{1\,0\,\bar{1}\,1\}\langle 1\,1\,\bar{2}\,0\rangle$, 12 $\langle c+a\rangle$ first order pyramidal slip systems $\{1\,0\,\bar{1}\,1\}\langle 1\,1\,\bar{2}\,3\rangle$ and six $\langle c+a\rangle$ second order pyramidal slip systems $\{1\,1\,\bar{2}\,2\}\langle 1\,1\,\bar{2}\,3\rangle$. The strongly anisotropic and orientation dependent plastic behavior of the α phase is due to the vastly different slip system resistances. The basal and prismatic $\langle a\rangle$ slip systems have the lowest resistance and are most favorable for slip activity, whereas the pyramidal $\langle c+a\rangle$ slip systems have the highest resistance showing no slip activity at room temperature. A transversely isotropic elastic tensor, with five independent constants, is used to model the elastic behavior of the α phase in these alloys. The β phase in these alloys have a cubic symmetry requiring three independent constants to model the elastic response and 48 slip systems divided into three families, $\{1\,1\,0\}\langle 1\,1\,1\rangle$, $\{1\,1\,0\}\langle 1\,1\,2\rangle$ and $\{1\,1\,0\}\langle 1\,2\,3\rangle$, to model the plastic response.

In crystal plasticity model, the total deformation gradient at a material point is multiplicatively split into an elastic and plastic part [6,7] as shown in Eq. (1). The elastic part of the deformation gradient $\mathbf{F^e}$ captures the stretching and rotation of the lattice. Plastic deformation happens through crystallographic slip on different slip systems and is captured through the evolution of the plastic deformation gradient $\mathbf{F^p}$ as shown in Eq. (2):

$$\mathbf{F}=\mathbf{F^e}\mathbf{F^p} \tag{1}$$

$$\dot{\mathbf{F}}^{\mathbf{p}}\mathbf{F}^{\mathbf{p}-\mathbf{1}}=\sum_{\alpha}\dot{\gamma}^{\alpha}\mathbf{S}_{\mathbf{0}}^{\alpha} \tag{2}$$

Here $\dot{\gamma}^{\alpha}$ is the slip rate on different slip systems and $\mathbf{S}_{\mathbf{0}}^{\alpha}$ is the Schmid tensor. The Schmid tensor is formed from the slip direction $\mathbf{m}_{\mathbf{0}}^{\alpha}$ and slip plane normal $\mathbf{n}_{\mathbf{0}}^{\alpha}$ in the reference configuration such that $\mathbf{S}_{\mathbf{0}}^{\alpha}=\mathbf{m}_{\mathbf{0}}^{\alpha}\otimes\mathbf{n}_{\mathbf{0}}^{\alpha}$. A power law is used to model slip rate on different slip systems as

$$\dot{\gamma}^{\alpha}=\dot{a}\left|\frac{\tau^{\alpha}-\chi^{\alpha}}{g^{\alpha}}\right|^{1/m} \tag{3}$$

Here $\dot{a}$ is a reference slip rate, τ^{α} is the resolved shear stress on the slip system, χ^{α} is the back stress, g^{α} is the slip system resistance and m is the power law exponent. The resolved shear stress on a slip system is related to the 2nd Piola–Kirchoff (PK2) stress as shown in Eq. (4). A hyper-elastic law is used to obtain the PK2 stress from the work conjugate Lagrange–Green strain tensor and is shown in Eq. (5). The evolution of slip system hardness is shown in Eq. (6) where h^{β} is the strain hardening rate due to self-hardening and $q^{\alpha\beta}$ is a matrix describing latent hardening. The evolution of back stress on a slip system depends on the slip rate on that slip system [21] and is shown in Eq. (7), where c and d are the direct hardening and dynamic recovery coefficient respectively:

$$\tau^{\alpha}=\mathbf{F^{eT}}\mathbf{F^{e}}\mathbf{T^{*}}:\frac{1}{2}(\mathbf{S}_{\mathbf{0}}^{\alpha}+\mathbf{S}_{\mathbf{0}}^{\alpha\mathbf{T}}) \tag{4}$$

$$\mathbf{T^{*}}=C:\mathbf{E^{e}}\quad\text{where }\mathbf{E^{e}}=\frac{1}{2}\left(\mathbf{F^{eT}}\mathbf{F^{e}}-\mathbf{I}\right) \tag{5}$$

$$\dot{g^\alpha} = \sum_\beta q^{\alpha\beta} h^\beta |\dot{\gamma^\beta}| \tag{6}$$

$$\dot{\chi^\alpha} = c\dot{\gamma^\alpha} - d\chi^\alpha |\dot{\gamma^\alpha}| \tag{7}$$

Different self-hardening relationships are used for the α and β phases. The evolution of self-hardening for the α phase is shown in Eq. (8) where h_0^α is the reference value of self-hardening and g_s^α is the saturation value of slip system resistance:

$$h^\alpha = h_0^\alpha \left|1 - \frac{g^\alpha}{g_s^\alpha}\right|^r \operatorname{sign}\left(1 - \frac{g^\alpha}{g_s^\alpha}\right)$$

$$g_s^\alpha = \tilde{g}\left|\frac{\dot{\gamma^\alpha}}{\dot{a}}\right|^c \tag{8}$$

The evolution of self-hardening of the β phase is shown in Eq. (9) where γ^{acc} is the accumulated plastic slip:

$$h^\alpha = h_s^\alpha + sech^2\left[\frac{h_0^\alpha - h_s^\alpha}{\tau_s^\alpha - \tau_0^\beta}\gamma^{acc}\right](h_0^\alpha - h_s^\alpha)$$

$$\gamma^{acc} = \int_0^t \sum_\alpha |\dot{\gamma^\alpha}|\, dt \tag{9}$$

The explicit modeling of the alternate lathe structure of the transformed $\alpha+\beta$ colonies for finite element simulations is computationally prohibitive. An equivalent homogenized model is developed in the work of Deka et al. [7] based on mixture rule for the colonies. The individual phases at a material point experiences the same deformation field but have independent evolution for the plastic variables and stresses. The stress at the material point is the weighted sum of the stresses in the individual phases in the colony as shown in Eq. (10). The weights correspond to the volume fractions of individual phases and depend on the chemical composition and processing conditions of these alloys:

$$\sigma = w_\alpha \sigma_\alpha + w_\beta \sigma_\beta \tag{10}$$

The effect of grain size and lathe thickness on the slip system resistance is also considered in the crystal plasticity model [9]. A Hall Petch type relation is used to modify the initial slip system resistances to capture the size effect as shown in Eq. (11), where D^α is a characteristic length parameter. For the globular α grains, the grain boundaries prevent transmission of dislocations to adjacent grains and resist further dislocation motion in these grains. Based on this observation, the grain diameter is considered as the characteristic length for these grains in Eq. (11). For the transformed $\alpha+\beta$ colonies, depending on the relative orientation of the lathe, dislocation motions can either be impeded by colony boundaries or lathe boundaries. Hence for the colonies, either the colony size or the lathe thickness is used in Eq. (11) to modify the initial slip system resistances:

$$g^\alpha = g_0^\alpha + \frac{K^\alpha}{\sqrt{D^\alpha}} \tag{11}$$

The different parameters in the modified crystal plasticity model are calibrated from experiments and finite element simulations of single crystal Ti-6Al and Ti-6242 [6,7,9]. Depending on the orientation of a grain relative to the loading direction, the amount of slip activity and extent of plasticity differs. A grain is identified as a soft grain if it has large amount of plastic deformation and as a hard grain if it has little or no plasticity [6]. From the finite element simulations under creep loading of polycrystalline Ti-alloys (Ti-6242,Ti-6Al) it is observed that stress concentration happens at the hard and soft grain interfaces. Also peak stress at the interface increases with the hold time of applied load. This phenomenon is known as *load shedding* and it arises from the condition of strain compatibility that needs to be satisfied at the interface [6]. This *load shedding* phenomenon is the driver for early crack initiation in Ti-alloys under dwell fatigue loading where there is an additional hold at maximum stress as compared to normal fatigue loading. To predict the number of cycles to crack initiation in polycrystalline Ti-alloys, crystal plasticity based finite element simulations under cyclic loading conditions have to be performed. Depending on the micro-structure and load characteristics, these simulations may have to be performed for large number of cycles and this can be computationally prohibitive. Use of accelerated time integration schemes can alleviate the problem and are discussed in the next section.

3. Accelerated time integration schemes

Finite element simulations of polycrystalline Ti-alloys under cyclic loading conditions for large number of cycles using conventional time integration scheme can be computationally prohibitive. The time steps used in conventional time stepping methods are constrained by the loading characteristics and response of crystal plasticity variables over a cycle. Since the crystal plasticity equations are strongly non-linear, small time steps are permitted for accuracy and convergence, at the onset of plasticity for each cycle. To overcome this challenge, a variety of accelerated time integration methods have been devised in the literature. An overview of some of the methods and their limitations for crystal plasticity models are discussed below.

3.1. Extrapolation based methods

In extrapolation based methods, single time scale cyclic simulations are performed for a few cycles and then the internal variables are extrapolated for large number of cycles based on them. High cycle fatigue problems have been studied in [22], where extrapolation is performed based on two complete strain cycles and response is assumed to stabilize thereafter. Fretting fatigue in titanium alloys also have been studied in [13,14] using this method. Fatigue life prediction of HSLA steels are performed by using crystal plasticity based finite element simulations and extrapolation based methods [15]. Functional relationships are derived for the local variables affecting the fatigue life in terms of number of cycles and macroscopically applied stress or strain.

The accuracy of extrapolation based methods is strongly dependent on the time or cycle from which extrapolation is performed and can be completely inaccurate and inefficient if stabilization of response happens after a large number of cycles [20]. Also these methods are macroscopic and cannot capture highly localized phenomenon like *load shedding* with sufficient accuracy. This pose as a major drawback of extrapolation based methods when used to predict highly localized event like crack initiation in Ti-alloys.

3.2. Multi-time scale methods

Under cyclic loading conditions, the response of crystal plasticity state variables, stresses and displacements has a high frequency fine time scale and a low frequency coarse time scale component. Hence multi-time scale methods can be used to decouple the responses so that integration is performed in the coarse time scale where the response is monotonic and significant benefit in computational time can be achieved. In dual time scale methods the coarse time t is related to the fine time τ by the relation $t = \varepsilon\tau$ where $\varepsilon \ll 1$ and forms the basis of decoupling the scales. Asymptotic expansion and almost periodic temporal homogenization (APTH) operator based multi-time scale methods have been used in [16–19] for performing decoupling in dissipative systems.

In asymptotic expansion based method [16–18], the response variables are expanded in an asymptotic series based on the different orders of contribution as shown in Eq. (12). The rate

equations and the corresponding initial conditions are modified accordingly as shown in Eq. (13):

$$y^{\zeta}(t) = y(t,\tau) = y_0(t,\tau) + \varepsilon y_1(t,\tau) + \varepsilon^2 y_2(t,\tau) + \cdots \tag{12}$$

$$\frac{dy^{\zeta}}{dt} = \frac{\partial y_0}{\partial t} + \frac{\partial y_1}{\partial \tau} + \frac{1}{\varepsilon}\frac{\partial y_0}{\partial \tau} + \varepsilon\left(\frac{\partial y_1}{\partial t} + \frac{\partial y_2}{\partial \tau}\right) + \cdots = f(y,t,\tau) \tag{13}$$

The assumption of local periodicity has been made in the work of Yu and Fish [16] which is not valid for evolving micro-structural variables in crystal plasticity simulations under cyclic loading. In the work of Ghosh et al. [17,18] this assumption has been relaxed and the variables are decomposed into cycle averaged and oscillatory components as shown in Eq. (14). The oscillatory response is further expanded in an asymptotic series as shown in Eq. (15):

$$y^{\zeta}(t) = y(t,\tau) = \overline{y}(t) + \tilde{y}(t,\tau) \quad \text{where } \overline{y}(t) = \frac{1}{T}\int_0^T y^{\zeta}(t)\,dt \tag{14}$$

$$\tilde{y}(t,\tau) = \tilde{y}_0(t,\tau) + \varepsilon\tilde{y}_1(t,\tau) + \varepsilon^2\tilde{y}_2(t,\tau) + \cdots \tag{15}$$

Effective constitutive equations are developed for the cycle-averaged problem by interpolating in a parameter space which is created by simulating two cycles of single slip system problems. Each order of oscillatory solution can be solved locally in temporal domain with the knowledge of the average solution. The method to obtain differential equations for different orders of oscillatory variable $\tilde{y}_n(t,\tau)$ is based on equating the different orders of contribution [17,18]. For crystal plasticity variables this yields the condition that the zeroth order oscillator of plastic deformation gradient is zero ($\tilde{\mathbf{F}}_0^{\mathbf{p}}(t,\tau) = 0$) and stress oscillators are elastic. This condition gets invalidated when stress ratio $R \to -1$ and there are large plastic oscillations. Thus asymptotic expansion methods cannot be used for problems when $R \to -1$. A detailed explanation of the drawbacks of asymptotic expansion based methods exemplified through a 1-D viscoplastic model is given in [20].

In APTH operator based dual scale method [19], the variables are assumed to evolve in an almost periodic manner. Such near periodicity can arise in constitutive laws due to damage or hardness evolution. The almost periodic variable is represented in terms of a periodic function and a small change which depends on the τ-scale as shown in Eq. (16). An almost periodic operator is defined such that it satisfies the condition of weak convergence similar to periodic fields and is shown in Eqs. (17) and (18). Although this method has no restriction for stress ratios as in asymptotic expansion based methods, it shows stability issues similar to explicit integration schemes owing to the staggered global–local approach used to solve the coarse scale initial boundary value problems [20]:

$$y_{ap}^{\zeta}(x,t) = y_{ap}(x,t,\tau) = y_p(x,t,\tau) + \zeta\tau\overline{y}(x) \tag{16}$$

$$\frac{\partial \mathfrak{M}(y_{ap})}{\partial t} = \frac{1}{T}\int_0^T \dot{y}_{ap}^{\zeta} dt \tag{17}$$

$$\lim_{\zeta\to 0}\int_{t^{\zeta}} y_{ap}^{\zeta}(x,t')\,dt' \to \int_t \mathfrak{M}(y_{ap}(x,t',\tau))\,dt' \tag{18}$$

The wavelet transformation based multi-time scale method used in this work overcomes the drawbacks of the existing multi-time scale methods to solve cyclic crystal plasticity problems and is described in the next section.

4. Wavelet transformation based multi-time scale method

The wavelet transformation based multi-time scale method is motivated by the dual time scale response of crystal plasticity variables subjected to cyclic loading (Fig. 1). As can be seen in Fig. 1(b), the large oscillations in the fine scale response constraints the time step that can be used in conventional single time scale integration algorithms. Performing fatigue simulations of real micro-structures for large number of cycles till crack initiation using such small time steps is computationally prohibitive. The objective is to decouple the fine and the coarse time scale responses so that integration is performed in the coarse time scale where the response is monotonic (Fig. 1(c)) and significant benefit in computational time can be achieved.

In this methodology the coarse time scale response is associated with the cycle scale and a kinematically admissible coarse scale displacement field $\mathbf{C}_k$ is sought at every coarse time N by minimizing the functional Π_c and is shown in Eq. (19). The coarse scale displacement field $\mathbf{C}_k(\mathbf{X},N)$ is a cyclic representation of the single time scale displacement field $\mathbf{u}(X,N,\tau)$. For dissipative systems, y_0 is the coarse scale representation of the evolving internal state variables:

$$\Pi_c = \Pi_c(\mathbf{x},\mathbf{C}_k,\mathbf{C}_k',y_0)$$

$$\mathbf{C}_k(\mathbf{x},N) | \delta\Pi_c(\mathbf{x},\mathbf{C}_k,\mathbf{C}_k',y_0) = 0$$

$$y_0(\mathbf{x},N) = y_0(\mathbf{x},N-\Delta N) + \int_{N-\Delta N}^{N} \frac{dy_0}{dN}(\mathbf{x},\mathbf{C}_k,\mathbf{C}_k',y_0)\,dN \tag{19}$$

A wavelet based transformation is used in the current methodology to linearly transform the displacement response over a cycle $\mathbf{u}(\mathbf{X},N,\tau)$ from the time domain to the wavelet space and is shown in Eq. (20). Here $\psi_k(\tau)$ are the wavelet basis functions and T is the period over which decomposition is performed. The time period of the loading cycle determines the period T:

$$\mathbf{C}_k(\mathbf{X},N) = \frac{1}{T}\int_0^T \mathbf{u}(\mathbf{X},N,\tau)\psi_k(\tau)\,d\tau \tag{20}$$

The wavelet coefficients $\mathbf{C}_k(\mathbf{X},N)$ show a monotonic response as compared to the normal displacement variable $\mathbf{u}(\mathbf{X},N,\tau)$ which shows large oscillations in the time domain. At any cycle the displacement

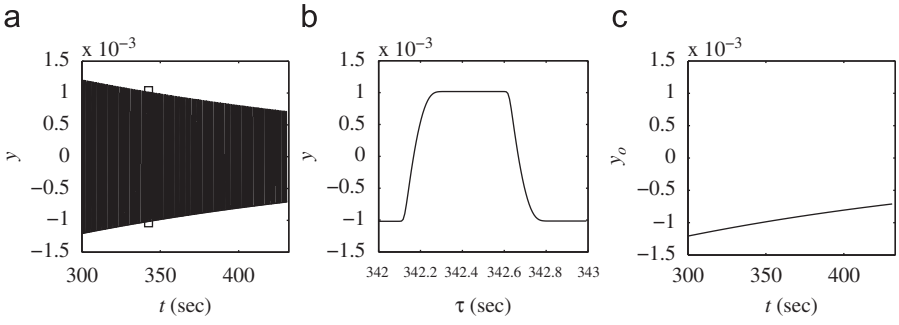

Fig. 1. Decoupling of crystal plasticity variables: (a) Single time scale response, (b) High frequency fine time scale response over one load period and (c) Coarse time/cycle scale evolution corresponding to the value at start of cycle.

response can be created once these coefficients are known as

$$\mathbf{u}(\mathbf{X},N,\tau) = \sum_{k=1}^{M} \mathbf{C}_k(\mathbf{X},N)\psi_k(\tau) \tag{21}$$

Here M is the number of wavelet basis functions required to accurately transform the waveform from the time domain to the wavelet space. For a discrete system M is determined from the resolution of the time domain over one period. The cyclic variation of deformation gradient at a material point can be constructed from the coefficients of displacement and is shown as

$$\mathbf{F}(\mathbf{X},N,\tau) = \mathbf{I} + \sum_{k=1}^{M} \frac{\partial \mathbf{C}_k}{\partial \mathbf{X}}(\mathbf{X},N)\psi_k(\tau) \tag{22}$$

As can be observed from Eq. (19), a coarse scale representation of the plastic variables is required to form the functional Π_c at any coarse time N. For a material point at cycle N, the evolution of plastic variables $y(\mathbf{X},N,\tau)$ and stress $\sigma(\mathbf{X},N,\tau)$ over the cycle can be obtained if the cyclic variation of deformation gradient $\mathbf{F}(X,N,\tau)$ and the initial value of crystal plasticity internal variables $y(\mathbf{X},N,\tau=0)$ are known and is shown in Eq. (23). Hence the initial values of crystal plasticity internal variables at every cycle are considered as the coarse scale internal variables ($y_0(\mathbf{X},N) = y(\mathbf{X},N,\tau=0)$).

$$y(\mathbf{X},N,\tau) = y_0(\mathbf{X},N) + \int_0^{\tau} \dot{y}(\mathbf{X},\tau',\mathbf{F}(\mathbf{X},N,\tau'))\, d\tau'$$

$$\sigma(\mathbf{X},N,\tau) = \hat{\sigma}(\mathbf{F}(\mathbf{X},N,\tau),y(\mathbf{X},N,\tau)) \tag{23}$$

Cycle scale rate equations are constructed for those internal variables which have a single time scale rate equation. From the crystal plasticity equations, the internal variables for which coarse scale rate equations are constructed are $\mathbf{F}^{\mathbf{p}}$, g^{α}, χ^{α} and γ^{acc}. The cycle scale rate equations for the internal variables $y_0(\mathbf{X},N) = y(\mathbf{X},N,\tau=0)$ are integrated using an implicit second order backward difference formula and is shown as

$$y_0(\mathbf{X},N+\Delta N) = \alpha_1 y_0(\mathbf{X},N) - \alpha_2 y_0(\mathbf{X},N-\Delta N_p) + \alpha_3 \frac{dy_0}{dN}(\mathbf{X},N+\Delta N)\Delta N$$

where

$$\alpha_1 = \frac{(r+1)^2}{(r+1)^2-1}, \quad \alpha_2 = \frac{1}{(r+1)^2-1}, \quad \alpha_3 = \frac{(r+1)^2-(r+1)}{(r+1)^2-1}$$

$$r = \frac{\Delta N}{\Delta N_p} \quad \Delta N \text{ and } \Delta N_p \text{ are the current and previous cycle} - \text{scale time steps} \tag{24}$$

The cyclic rate of change of the coarse scale variable $y_0(\mathbf{X},N)$ at cycle N is defined as the evolution of the variable $y(\mathbf{X},N,\tau)$ over that cycle and is shown in Eqs. (25) and (26). The cyclic integration of crystal plasticity equations shown in (26) is performed numerically using backward Euler scheme at suitable time points [5]:

$$\frac{dy_0}{dN}(\mathbf{X},N) = y(\mathbf{X},N,T) - y_0(\mathbf{x},N) \tag{25}$$

$$y(\mathbf{X},N,T) = y_0(\mathbf{X},N) + \int_0^{T} \dot{y}(\mathbf{X},,\tau,\mathbf{F}(\mathbf{X},N,\tau))\, d\tau \tag{26}$$

The wavelet based transformation of the displacement variables over a cycle in conjunction with the implicit second order backward difference scheme for the cycle scale internal variables provides a consistent framework of integration for the coarse scale variables. Due to the implicit nature of integration, the method does not have stability issues as present in APTH operator based multi-time scale method. Moreover the technique does not have assumptions on the order of contribution as present in asymptotic expansion based multi-time scale method. Thus this methodology works for all stress ratios as opposed to the asymptotic expansion based methods which fails when the stress ratio $R \to -1$. The selection of proper basis functions for decomposition of the displacement response over a cycle is important for the convergence of the cycle scale boundary value problem. It should also reduce the number of displacement coefficients that needs to be solved to provide computational benefit. The wavelet basis functions have these desirable properties and hence considered in this method. The next section gives an overview on wavelets and discusses about some of its properties which makes it appropriate for this work.

4.1. Wavelets overview

Wavelet transformation of functions $f \in L^2(R)$ introduces scaling function ϕ which spans the space of square integrable functions through its translation and dilation as

$$f(\tau) = \sum_{m=1}^{M_{res}} \sum_{n=1}^{N_{trans}} C_{mn} 2^{m/2} \phi(2^m \tau - n) \tag{27}$$

Here M_{res} is the number of resolutions (dilations) and N_{trans} is the number of translation in each resolution. The scaling function has the property of compact support i.e., non-zero within a defined span and the span size s depends on the type of wavelets used. For example for Haar wavelets $s \in [0,1)$ whereas for Daubechies-4 wavelets $s \in [0,3)$. The scaling functions also satisfy the refinement condition which relates the scaling functions at a higher resolution to the scaling functions at a lower resolution and is shown as

$$\phi(\tau) = \sum_{k=1}^{N_{filter}} h_k \phi(2\tau - k) \tag{28}$$

Here the parameters h_k and N_{filter} depend on the type of wavelet basis. The scaling functions can be used to produce a nested sequence of subspaces at different resolutions as shown in Eq. (29). The nested sequence of functions f_m obtained by projection at different subspaces V_m are the approximations to the original function f at different resolution levels. This multi-resolution property yields a complimentary space and is the detail space W_m. The detail space is the orthogonal difference between two consecutive resolutions V_m and V_{m+1}. The wavelet basis function have compact support and satisfy refinement condition similar to the scaling functions and is shown in Eq. (30):

$$0 \subset \cdots \subset V_0 \subset V_1 \subset \cdots \subset V_m \subset V_{m+1} \subset \cdots \subset L^2(R) \tag{29}$$

$$\psi(\tau) = \sum_{k=1}^{N_{filter}} g_k \phi(2\tau - k) \tag{30}$$

The integration of crystal plasticity equations is performed at discrete time points and hence discrete wavelet transforms are used for decomposing and reconstructing displacement responses. The transformation can be achieved through a recursive projection of the original function into approximate and detail spaces at coarser resolutions and is shown as

$$\begin{aligned} f^m(\tau) &= \sum_n \langle f^m, \phi_{m-1,n} \rangle \phi_{m-1,n} + \sum_n \langle f^m, \psi_{m-1,n} \rangle \psi_{m-1,n} \\ &= \sum_n a^{m-1,n} \phi_{m-1,n} + \sum_n d^{m-1,n} \psi_{m-1,n} \\ &= f^{m-1} + \sum_n d^{m-1,n} \psi_{m-1,n} \end{aligned} \tag{31}$$

Here m is the resolution and n is the translation in the corresponding resolution. The original function $f^m(\tau)$ consists of uniformly spaced points and the maximum resolution is governed by the minimum time step that is required to integrate the crystal plasticity equations. The recursive procedure yields approximate coefficients $a^{0,n} \in V_0$ and detail coefficients $d^{l,n} \in W_l$ where $l \in [0, m-1]$. This multi-resolution property of wavelet transformation can be used to retain coefficients where response variations are high and eliminate coefficients where changes are slow.

The discrete wavelet transformation can be performed through matrix operation where the transformation matrix $\mathbf{T}$ is created from the low pass filters h_k and high pass filters g_k [20,23]. The filter coefficients arise from the refinement conditions shown in Eqs. (28) and (30). The transformation matrix $\mathbf{T}$ is orthogonal and sparse. The sparsity property can be used to obtain computational benefit when decomposition and reconstruction of displacement responses are performed using the transformation matrix. The properties of wavelet basis that are advantageous and hence justify its use in this work are summarized below.

- *Compact support*: Each wavelet basis spans a finite domain and hence does not exhibit spurious instabilities like Gibb's phenomenon associated due to truncation of infinite series as in Fourier series representations.
- *Multi-resolution*: At different resolutions the set of basis functions is finite and known a priori unlike Fourier series where this is found by trial and error.
- *Projection in time and frequency domain*: Since wavelet transformation performs projection in both time and frequency domain unlike Fourier transform, it enables the reduction of the number of coefficients required to be solved to a larger extent than Fourier transform.

4.2. Coarse scale finite element framework

In non-linear initial boundary value problems, temporal integration is performed at discrete time points and the spatially discretized domain is equilibrated in a weak sense at each time point τ_n. The equilibrated displacement field $\mathbf{u}(\mathbf{X},\tau_n)$ is obtained by solving the residual equations shown in Eq. (32), in an iterative scheme at each time point. The equilibration of a cycle implies that the residual equations are satisfied at each discrete time point τ_n constituting that cycle and is shown in Eq. (33):

$$\mathbf{f}(\tau_n)=\sum_{el}\int_{\Omega_n^{el}}\mathbf{B}^{\mathbf{T}}(\tau_n)\sigma(\tau_n)\,d\Omega_n^{el}-\int_{\Gamma_n}\mathbf{N}^{\mathbf{T}}\mathbf{t}(\tau_n)\,d\Gamma_n=0 \tag{32}$$

$$\mathbf{f}(\tau_n)=0 \quad \forall\tau_n\in[0,T] \tag{33}$$

To solve the coarse scale boundary value problem, a modified finite element method is devised where the wavelet coefficients of displacement variables $\mathbf{C}_k(\mathbf{X},M)$ are the primary variables. The residual equations for any coarse scale cycle M are obtained by transforming the residual equations at each discrete τ_n within the cycle into the wavelet space and are shown in Eq. (34). For the cycle to be in equilibrium all the wavelet coefficients of residual must satisfy the condition shown in Eq. (35):

$$\mathbf{R}_k(M)=T_{kl}\mathbf{f}(M,\tau_l)=T_{kl}\left(\sum_{el}\int_{\Omega_l^{el}}\mathbf{B}^{\mathbf{T}}(M,\tau_l)\sigma(M,\tau_l)\,d\Omega_l^{el}-\int_{\Gamma_l}\mathbf{N}^{\mathbf{T}}(M,\tau_l)\mathbf{t}(\tau_l)\,d\Gamma_l\right) \tag{34}$$

$$\mathbf{R}_k(M)=T_{kl}\mathbf{f}(M,\tau_l)=0 \tag{35}$$

The wavelet coefficients of residual $\mathbf{R}_k(\mathbf{X},M)$ for cycle M depend on the wavelet coefficients of displacement $\mathbf{C}_k(\mathbf{X},M)$. The equilibrated field of wavelet coefficients of displacement is obtained by iteratively solving the modified residual equations using Newton's Method. The linearization of the modified residual equations and iterative update of the wavelet coefficients of displacement are shown as

$$\mathbf{R}_k(\mathbf{C_l})|_{i+1}=\mathbf{R}_k(\mathbf{C_l})|_i+\left.\frac{\partial\mathbf{R}_k}{\partial\mathbf{C_l}}\right|_i\Delta\mathbf{C_l}|_i$$

$$\mathbf{R}_k(\mathbf{C_l})|_{i+1}=0\Rightarrow\Delta\mathbf{C_l}|_i=-\left[\left.\frac{\partial\mathbf{R}_k}{\partial\mathbf{C_l}}\right|_i\right]^{-1}\mathbf{R}_k(\mathbf{C_l})|_i$$

$$\mathbf{C_l}|_{i+1}=\mathbf{C_l}|_i+\Delta\mathbf{C_l}|_i \tag{36}$$

For a given initial-boundary value problem, the spatial discretization of the coarse scale finite element model is same as the single time scale model. However the global degrees of freedom in this method increases, since at every coarse time scale increment (cycle), the wavelet coefficients required to represent the cyclic nodal displacement response is solved. Similarly, the size of the tangent stiffness matrix of the modified finite element problem also increases by square of this factor. The computation and factorization of the tangent stiffness matrix at every cyclic increment can hinder the performance of this method. To avoid this problem, a quasi-Newton method is used where an approximate tangent stiffness matrix is evaluated and factored in the first coarse time increment and used in the subsequent increments. Reformations of the approximate tangent stiffness matrix are performed if convergence is not achieved after a prescribed number of iterations. The approximate tangent stiffness matrix $\tilde{\mathbf{K}}_\mathbf{c}$ is shown in Eq. (37), where $\mathbf{K}$ is the tangent stiffness matrix at each discrete time point τ_n within the cycle and $\mathbf{T}$ is the transformation matrix discussed in Section 4.1. The global tangent stiffness matrix is updated using a Broyden scheme. Due to the monotonic behavior of the coarse scale response such an approximation works well without convergence issues:

$$[\tilde{\mathbf{K}}_\mathbf{c}]_{kl}=T_{kn}[\mathbf{K}(\tau_n)]T_{nl} \tag{37}$$

The initial condition of the plastic variables and initial guess of the wavelet coefficients in the coarse scale finite element method are obtained by simulating few cycles of fine scale. For dwell cyclic problems, with large hold period, fine scale simulations with constant time steps based on maximum resolution are very inefficient [20]. To alleviate this problem, the total time period is split into different segments with different maximum resolutions. Automatic time stepping in multiples of 2 is performed within each segment to accelerate the first few cycles of fine scale simulation. This also ensures that 2^n number of time points are obtained in each segment and a wavelet transformation of the cyclic displacement can be performed as

$$\mathcal{I}=\bigcup_{j=1}^{\mathcal{N}_{seg}}\mathcal{I}_{seg}^j \quad \text{where } \mathcal{N}_{seg}=\text{no. of segments}$$

$$\mathcal{I}_{seg}^j=\{\mathbf{C}_k(N)|\mathbf{C}_k(N)=T_{kl}^j\mathbf{u}(\mathbf{X},N,\tau_l^j)\}\quad\forall\tau_l^j\in[\tau_{seg}^{j-1},\tau_{seg}^j) \tag{38}$$

The initial guess of the plastic variables and wavelet coefficients are improved for better convergence rate. A second order extrapolation is done based on the previous cycle values and gradients as

$$\mathbf{C}_k(N+\Delta N)=(1+\alpha_1+\alpha_2)\mathbf{C}_k(N)-\alpha_1\mathbf{C}_k(N-\Delta N_p)-\alpha_2\mathbf{C}_k(N_p-r_p\Delta N_p)$$

$$y_0(N+\Delta N)=\beta_1 y_0(N)+\beta_2 y_0(N-\Delta N_p)+\beta_3\frac{dy_0}{dN}(N)\Delta N$$

where

$$\alpha_1=\frac{r(r_p+1)+1}{r_p r^2},\quad \alpha_2=-\frac{r+1}{r_p(r_p+1)r^2}$$

$$\beta_1=\frac{r^2-1}{r^2},\quad \beta_2=\frac{1}{r^2},\quad \beta_3=\frac{r^2+r}{r^2},\quad r=\frac{\Delta N_p}{\Delta N},\quad r_p=\frac{\Delta N_p'}{\Delta N_p}$$

ΔN, ΔN_p, $\Delta N_p'$ are the current and two previous cycle jumps (39)

In the wavelet transformation based multi-time scale method the cyclic description of the displacement field in the wavelet space increases the size of the problem. To reduce the size of the problem, only the evolving coefficients are considered in the global set of equations. However the displacement waveform can change shape as the problem progresses. Hence the use of a fixed set of displacement coefficients from the start of the simulation can cause divergence and inaccuracy in the solution. Adaptive criteria are developed to add the evolving coefficients and remove the non-evolving coefficients. The use of adaptive criteria at the

start of each cyclic increment keeps the optimal number of degrees of freedom that is solved and avoids divergence and inaccuracy in the solution [20]. In this adaptive criteria the total set of wavelet coefficients $\mathcal{I}=\{\mathbf{C}_k|k=1..N_{wav}\}$, where N_{wav} is the total number of coefficients, is divided into a set of evolving $\mathcal{I}^{evol}$ and non-evolving $\mathcal{I}^{non\text{-}evol}$ coefficients, i.e. $\mathcal{I}=\mathcal{I}^{evol}\bigcup\mathcal{I}^{non\text{-}evol}$. The set of evolving coefficients at each cyclic increment is selected from the wavelet space by observing the change of the coefficients at each resolution and is shown in Eq. (40). The set of non-evolving coefficients is obtained as shown in Eq. (41):

$$\mathcal{I}=\{\mathbf{C}_k|\mathbf{C}_{k+1}-2\mathbf{C}_k+\mathbf{C}_{k-1}>\eta C_k^{tol},k=1..N_{wav}\}=\{\hat{\mathbf{C}}_k|k=1..N_{evol}\} \tag{40}$$

$$\mathcal{I}^{non\text{-}evol}=\mathcal{I}-\mathcal{I}^{evol} \tag{41}$$

An automatic coarse scale time stepping criterion, which corresponds to the number of cycles traversed in each increment of the numerical integration scheme, is also devised [20]. The optimal step size is estimated from the truncation error of the coarse scale plastic deformation gradient $\mathbf{F}_0^{\mathbf{p}}$ in conjunction with the residual of the equilibrium equation. For the implicit second order backward difference scheme, the truncation error is derived from the truncation of second order terms in Taylor's series expansion as shown in Eq. (42). The effect of the local constitutive level integration error on the global equilibrium equations in the coarse scale problem is shown in Eq. (43). For the error to be bounded by a prescribed relative tolerance η, the maximum allowed cycle step jump ΔN is estimated from Eq. (44):

$$\delta\mathbf{F}_0^{\mathbf{p}}=\frac{1}{6}\left|\frac{d^3\mathbf{F}_0^{\mathbf{p}}}{dN^3}\frac{(r+1)^2-(r+1)^3}{(r+1)^2-1}\right|\Delta N^3 \tag{42}$$

$$\delta f_{err}=\frac{1}{6}\left\|\int_{\Omega_{el}}\mathbf{B}^{\mathbf{T}}\frac{\partial\sigma}{\partial\mathbf{F}_0^{\mathbf{p}}}\frac{(r+1)^2-(r+1)^3}{(r+1)^2-1}\frac{d^3\mathbf{F}_0^{\mathbf{p}}}{dN^3}d\Omega_{el}\right\|\Delta N^3 \tag{43}$$

$$\Delta N\le\left(\frac{6\eta\tilde{f_{err}}}{\delta f_{err}}\right)^{1/3}\quad\text{where }\tilde{f_{err}}=\sum_{el}\left\|\int_{\Omega_{el}}\mathbf{B}^{\mathbf{T}}\frac{\partial\sigma}{\partial\mathbf{F}_0^{\mathbf{p}}}d\Omega_{el}\right\| \tag{44}$$

5. Dwell fatigue simulations using wavelet transformation based multi-time scale method

Crystal plasticity FE simulation using the wavelet transformation based multi-time scale method is performed on a representative Ti–6Al sample to illustrate the accuracy and computational efficiency of the developed methodology. The dimensions of the sample are 14 μm × 14 μm × 14 μm and the micro-structure consists of 343 grains with different orientations. A follower load is applied on the *y*-face of the sample. The initial *c*-axis orientation of the grains and the *c*-axis orientation distribution of the sample is shown in Fig. 2. The follower load is a dwell cyclic load with a maximum applied macroscopic traction of 700 MPa and a minimum of 0 MPa. The total time period of the dwell load is 122 s, which comprises a hold time of 120 s, a loading and unloading time of 1 s each. The coarse scale simulation of this sample using the proposed methodology is started from the 21st cycle. Fine scale simulations are performed for the first 20 cycles and the initial condition of the plastic variables and the initial guess of the wavelet coefficients are obtained from it (Section 4.2). Daubechies-4 wavelets are used for transformation [20] since it satisfies the 1st moment conditions and requires less number of coefficients to represent the almost linear portions of the nodal displacement response. The initial set of evolving coefficients are chosen based on Eq. (40). The initial coarse scale time step is $\Delta N=1$. The subsequent cycle jumps are selected based on the criterion discussed in Section 4.2.

To compare the accuracy of the proposed methodology, fine scale simulations are continued till 170th cycle. The evolution of the initial value of plastic deformation gradient component $\mathbf{F}_{0,22}^{\mathbf{p}}$ and slip system hardness g^{α} at a material point is compared as shown in Fig. 3. The distribution of stress component σ_{yy} in the sample is plotted for 156th cycle at 121st second in Fig. 4. As can be observed from Figs. 3 and 4, the coarse and fine scale results show excellent agreement. Hence the method can be used for failure predictions in these alloys where the accuracy of evolution of micro-structural variables is of utmost importance.

To estimate the computational benefit of the proposed methodology, the coarse scale simulation is performed for 100,000 cycles. The evolution of initial value of plastic deformation gradient component $\mathbf{F}_{0,22}^{\mathbf{p}}$ at a material point is shown in Fig. 5. As can be observed from the figure, the coarse scale time steps (cycle jumps) increase as the simulation progresses and significant computational advantage is obtained. To calculate the time advantage of this method, the total time for the coarse scale simulation is obtained from $t_c=t_1+t_2$ where t_1 is the time taken for the first 20 cycles of fine scale simulation and t_2 is the time of coarse scale simulation. The total time of fine scale simulation t_f for N_f=100,000 cycles is obtained by extrapolating the time t_n required to complete N_n=170 cycles and is shown in Eq. (45). A computational benefit of ~200 times is achieved for the given problem:

$$t_f=\frac{N_f}{N_n}t_n \tag{45}$$

The evolution of stress σ_{yy} along a material line for the 21st cycle and 100,000th cycle at 121st second is shown in Fig. 6.

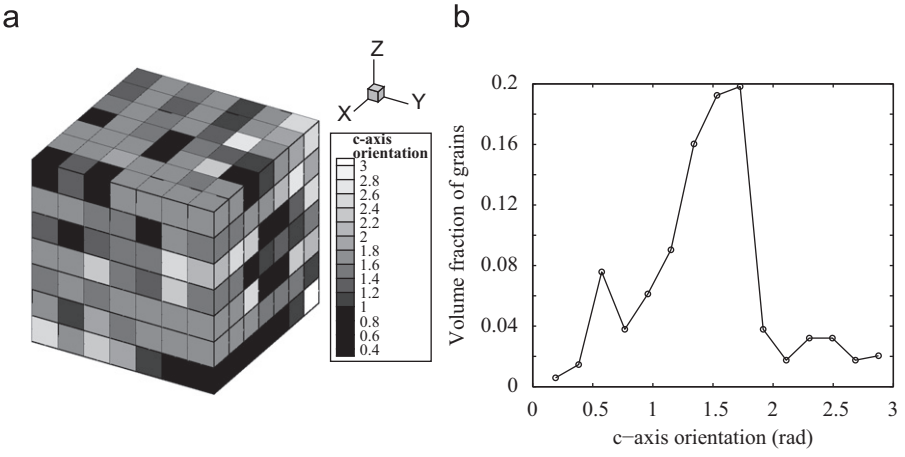

Fig. 2. *c*-Axis orientation: (a) *c*-Axis orientation of individual grains in the sample and (b) *c*-Axis orientation distribution of the representative micro-structure.

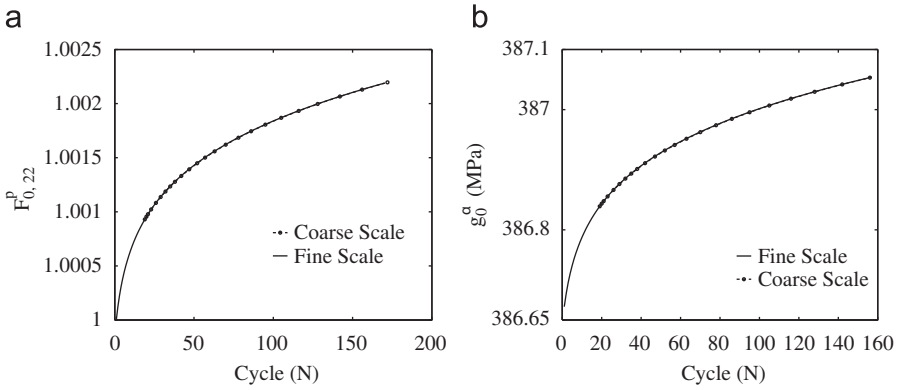

Fig. 3. Comparison of evolution of initial value of plastic variables y_0 at a material point: (a) $\mathbf{F}^{\mathbf{p}}_{0,22}$ component and (b) g^{α}_{0} of a slip system.

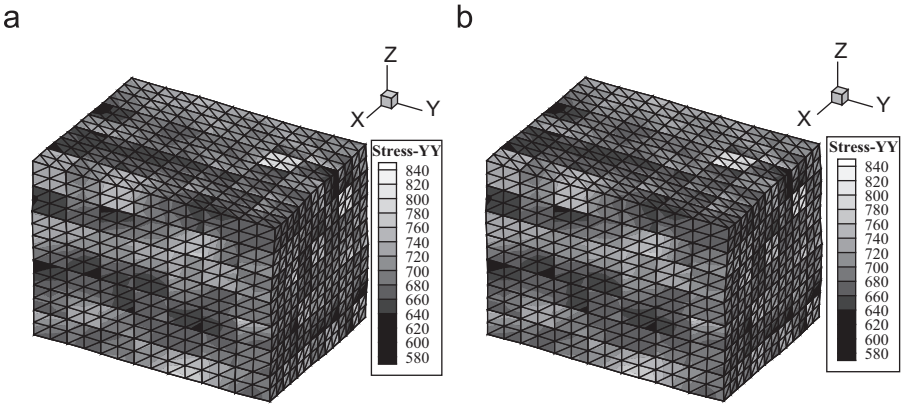

Fig. 4. Stress σ_{yy} distribution in the micro-structure at 156th cycle and 121st second: (a) Wavelet transformation based multi-time scale simulation and (b) Fine scale simulation.

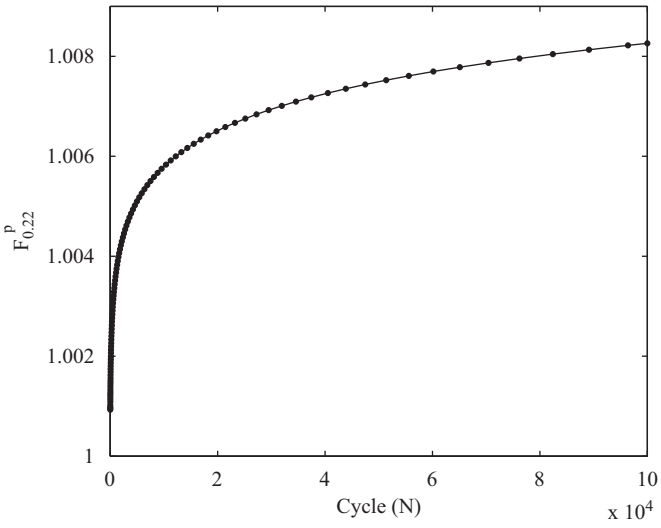

Fig. 5. Evolution of plastic deformation gradient component $\mathbf{F}^{\mathbf{p}}_{\mathbf{0},22}$ at a material point

The phenomenon of *load shedding* associated with inhomogenous plastic flow in Ti-alloys is clearly visible. As discussed in Section 2, this stress concentrations are the primary driver for early crack nucleation in these alloys. From Fig. 6(b) it can also be observed that the stress peak rises with cycles which makes the micro-structure more susceptible to failure.

6. Conclusion

This paper describes a wavelet transformation based multi-time scaling method for crystal plasticity finite element simulations of dwell cyclic deformation in Titanium alloys leading to fatigue failure. Multi-time scaling is motivated by the large number of cycles that may be required to initiate a fatigue crack in these samples. Simulating such large number of cycles remains intractable to conventional single time scale finite element analysis. The unique aspect of this methodology is that the algorithm does not assume scale separation as with other conventional multi-time scale methods.

The wavelet transformation based multi-time scale methodology introduces wavelet decomposition of nodal displacements and cycle scale rate equations of all associated plastic variables in the finite element formulation, to decouple the response into a monotonic coarse cycle-scale behavior and a oscillatory fine time scale behavior. Multi-resolution wavelet basis functions can effectively capture the rapidly varying fine scale response, which necessitates very small time steps in conventional single time scale FEM simulations. Criteria for selecting the optimal number of wavelet coefficients in the representation of nodal displacement functions and selecting appropriate coarse scale time steps in the crystal plasticity simulations is used.

Coarse scale variables exhibit monotonic behavior, that stabilizes with saturating hardness at higher levels of deformation. Relatively large increments, traversing several cycles at a time, can therefore be utilized in the numerical integration scheme with significantly enhanced efficiency. A 3-D crystal plasticity model for

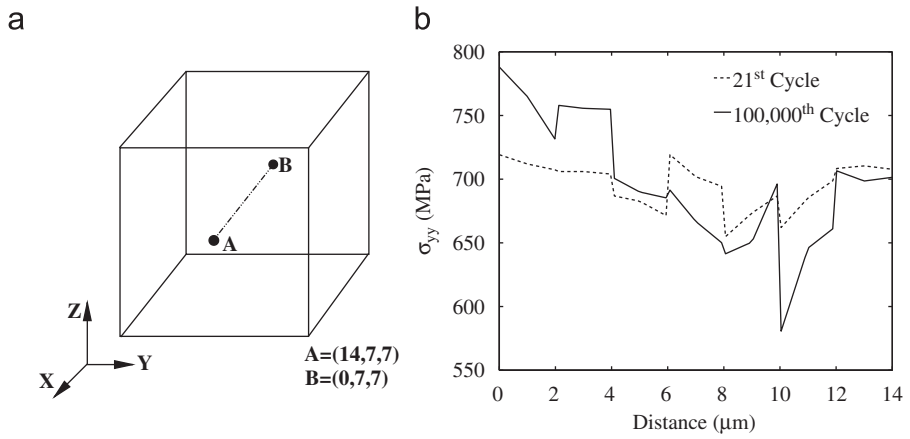

Fig. 6. Stress σ_{yy} distribution in the micro-structure along a material line: (a) The material line across which σ_{yy} distribution is considered and (b) Stress σ_{yy} distribution.

a representative Ti–6Al with dwell cyclic loading conditions is simulated using the wavelet transformation based multi-time scale method. The results are in excellent agreement with that of single time scale FEM simulations, while obtaining approximately 200 times speed-up for 100,000 cycles. Subsequently, fine scale variations in temporal response at any point in a micro-structural point can be recovered from values of the nodal displacement wavelet coefficients and the coarse scale state variables at that point. Such fine scale information on micro-structural state variables is required in predicting crack nucleation in the micro-structure.

Acknowledgments

This work has been supported by the US National Science Foundation (Grant # CMMI-0800587, Program Manager: Dr. Clark Cooper), and Air Force office of Scientific Research (DCT Grant # FA-9550-09-1-045 2, Program Manager: Dr. David Stargel). This sponsorship is gratefully acknowledged. Computer support by the Ohio Supercomputer Center through Grant PAS813-2 is also gratefully acknowledged.

References

[1] J.G. Lutjering, J.C. Williams, Titanium, second ed., Springer, Berlin, Heidelberg, New York, 2007.
[2] S. Suresh, Fatigue of Materials, Cambridge University Press, Cambridge, 1998.
[3] L.F. Coffin, Fatigue, Ann. Rev. Mater. 2 (1973) 313–348.
[4] P.C. Paris, The fracture mechanics approach to fatigue, Fatigue—An Interdisciplinary Approach, Syracuse University Press, Syracuse, 1964.
[5] S. Kalidindi, C. Bronkhorst, L. Anand, Crystallographic texture evolution in bulk deformation processing of fcc metals, J. Mech. Phys. Solids 40 (1992) 537–569.
[6] V. Hasija, S. Ghosh, M. Mills, D. Joseph, Modeling deformation and creep in Ti–6Al alloys with experimental validation, Acta Mater. 51 (2003) 4533–4549.
[7] D. Deka, D. Joseph, S. Ghosh, M. Mills, Crystal plasticity modeling of deformation and creep in polycrystalline Ti-6242, Metall. Trans. A 37 (5) (2006) 1371–1388.
[8] G. Venkatramani, D. Deka, S. Ghosh, Crystal plasticity based FE model for understanding microstructural effects on creep and dwell fatigue in Ti-6242, ASME J. Eng. Mater. Technol. 128 (3) (2006) 356–365.
[9] G. Venkataramani, S. Ghosh, M. Mills, A size dependent crystal plasticity finite element model for creep and load-shedding in polycrystalline Titanium alloys, Acta Mater. 55 (2007) 3971–3986.
[10] G. Venkataramani, K. Kirane, S. Ghosh, Microstructural parameters affecting creep induced load shedding in Ti-6242 by a size dependent crystal plasticity FE model, Int. J. Plasticity 24 (2008) 428–454.
[11] K. Kirane, S. Ghosh, A cold dwell fatigue crack nucleation criterion for polycrystalline Ti-6242 using grain-level crystal plasticity FE model, Int. J. Fatigue 30 (2008) 2127–2139.
[12] K. Bathe, Finite Element Procedures, Prentice-Hall, 1995.
[13] C. Goh, J. Wallace, R. Neu, D. McDowell, Polycrystal plasticity simulations of fretting fatigue, Int. J. Fatigue 23 (2001) 5423–5435.
[14] C. Goh, R. Neu, D. McDowell, Crystallographic plasticity in fretting of Ti–6Al–4V, Int. J. Plasticity 19 (2003) 1627–1650.
[15] S. Sinha, S. Ghosh, Modeling cyclic ratcheting based fatigue life of HSLA steels using crystal plasticity FEM simulations and experiments, Int. J. Fatigue 28 (2006) 1690–1704.
[16] Q. Yu, J. Fish, Temporal homogenization of viscoelastic and viscoplastic solids subjected to locally periodic loading, Comput. Mech. 29 (2002) 199–211.
[17] S. Manchiraju, M. Asai, S. Ghosh, A dual time scale finite element model for simulating cyclic deformation of polycrystalline alloys, J. Strain Anal. Eng. Des. 42 (2007) 183–200.
[18] S. Manchiraju, K. Kirane, S. Ghosh, Dual-time scale crystal plasticity FE model for cyclic deformation of Ti alloys, J. Comput. Aided Mater. Des. 14 (2008) 47–61.
[19] C. Oskay, J. Fish, Multiscale modeling of fatigue for ductile materials, Int. J. Multiscale Comput. Eng. 2 (2004) 1–25.
[20] D. Joseph, P. Chakraborty, S. Ghosh, Wavelet transformation based multi-time scaling for crystal plasticity FE simulations under cyclic loading, Comput. Methods Appl. Mech. Eng. 199 (2010) 2177–2194.
[21] R. Morrissey, D. McDowell, T. Nicholas, Microplasticity in HCF of Ti–6Al–4V, Int. J. Fatigue 23 (2001) S55–S64.
[22] V. Bennett, D. McDowell, Polycrystal orientation distribution effects on microslip in high cycle fatigue, Int. J. Fatigue 25 (2003) 27–39.
[23] G. Strang, T. Nguyen, Wavelets and Filter Banks, Wellessey College, 1996.